CONF-961105--16
SAND96-1468C
SAND--96-1468C

Modeling Delamination Growth in Composites

E. D. Reedy, Jr. and F. J. Mello
Sandia National Laboratories
Albuquerque, New Mexico 87185

Abstract

A method for modeling the initiation and growth of discrete delaminations in shell-like composite structures is presented. The laminate is divided into two or more sublaminates, with each sublaminate modeled with four-noded quadrilateral shell elements. A special, eight-noded hex constraint element connects opposing sublaminate shell elements. It supplies the nodal forces and moments needed to make the two opposing shell elements act as a single shell element until a prescribed failure criterion is satisfied. Once the failure criterion is attained, the connection is broken, creating or growing a discrete delamination. This approach has been implemented in a three-dimensional finite element code. This code uses explicit time integration, and can analyze shell-like structures subjected to large deformations and complex contact conditions. The shell elements can use existing composite material models that include in-plane laminate failure modes. This analysis capability was developed to perform crashworthiness studies of composite structures, and is useful whenever there is a need to estimate peak loads, energy absorption, or the final shape of a highly deformed composite structure.

This paper describes the eight-noded hex constraint element used to model the initiation and growth of a delamination, and discusses associated implementation issues. Particular attention is focused on the delamination growth criterion, and it is verified that calculated results do not depend on element size. In addition, results for double cantilever beam and end notched flexure specimens are presented and compared to measured data to assess the ability of the present approach to model a growing delamination.

Acknowledgment- The work was performed at Sandia National Laboratories and supported by the U. S. Department of Energy under contract DE-AC04-94AL85000.

DISCLAIMER

Introduction

This work focuses on modeling the initiation and growth of discrete delaminations. Even a single delamination can have a dramatic effect on the flexural stiffness of a laminated composite. For example, if a homogeneous beam is split in half, the flexural stiffness is reduced to 25% of its original value. If instead the beam is split into three beams, the stiffness is reduced to 11% of its original value. Accordingly, an analysis that includes the initiation and growth of just one or two discrete delaminations, located at a depth where they have the greatest impact on flexural stiffness, is expected to provide a reasonable representation of a delaminated composite. This is the approach taken in the present work. The laminate is broken up into two or more sublaminates. Each sublaminate is modeled with four-noded quadrilateral shell elements. The shell elements can be layered, and can use existing composite material models that include the in-plane failure modes of interest. A special, eight -noded hex constraint element connects opposing sublaminate shell elements, and supplies the nodal forces and moments needed to make the two opposing shell elements act as a single shell element until a prescribed failure criterion is satisfied. The connection is then broken, creating or growing a discrete delamination.

The efficacy of an analysis that uses a partially bonded assemblage of plate-like sublaminates to model a laminate with a fixed, preexisting delamination is well established. [1-4]. There have also been several efforts aimed at extending this type of analysis to a growing delamination. For example, Sankar and Hu [5] connect linear elastic beam elements with extensional and torsional springs that fail when the energy release rate reaches a critical value. They analyzed impact induced growth of a preexisting delamination embedded within a cantilevered beam. Farley and Jones [6] model delamination by disconnecting "zero length" extensional and torsional springs between coincident nodes of adjacent shell elements when the energy release rate reaches a critical value. Their large deformation analysis uses a nonlinear elastic idealization with a maximum strain failure criterion for the in-plane material model. A small section of a composite tube was modeled to estimate sustained crushing stress. Song and Waas [7] use a linear elastic beam on a

nonlinear spring foundation to model delamination growth in a double cantilever beam fracture specimen. A spring fails when the total strain energy in the spring reaches a critical value.

Notable features of the present analysis include 1) a three-dimensional, large deformation capability, 2) modeling the initiation and growth of one or more discrete delaminations, 3) compatibility with existing shell element formulations, in-plane material models, and mesh generation tools, and 4) implementation in a finite element code that uses explicit time integration to advance the equations of motion from the initial state. Note that explicit finite element codes, sometimes referred to as "wave codes", are used to solve transient dynamic problems that include highly nonlinear material response and large deformations [8]. They are also used for quasistatic loadings when the model contains a large number of elements, complex contact conditions, geometric instabilities, or material softening. In the following, the approach for modeling discrete delaminations is reviewed, implementation issues are discussed, and illustrative examples are presented.

Approach for Modeling Discrete Delaminations

The basic idea is easily visualized by considering a 2D representation. The laminate is broken into two shells (sublaminates) of thickness h, with nodes located along each shell's mid-surface. Focus attention on the two nodes on the left hand side of two opposing elements (Fig. 1a). The relative normal (mode I) displacement across the connection plane (the location of a potential delamination) is simply equal to the relative nodal displacement in the normal direction (the shells are inextensible in the thickness direction). The relative tangential (mode II) displacement across the connection plane is based on the displacement at the bottom of the top shell and that on the top of the bottom shell. As indicated in Fig. 2a, these displacements can be defined in terms of the tangential nodal displacement and nodal rotation defined at the shell's mid-surface. To make the two shells act as one, the relative displacements across the connection plane (ΔU_j and ΔV_j) must be constrained or penalized to enforce an acceptable level of displacement continuity. The penalty parameter (i.e., K_n or K_t) can be thought of as a spring constant that is applied to the relative dis-

placement, and the stiffer the spring the more precisely the constraint is enforced. The associated forces act on the connection plane and correspond to the internal forces that hold the sublaminates together prior to delamination (Figs. 1b, 2b). These forces are then replaced by equivalent nodal forces and moments (Figs. 1c, 2c). Note that the corresponding nodal degrees of freedom on opposite sides of the delamination plane are not simply tied together. There are no torsional springs, nor are there concentrated moments on the delamination plane. The present approach produces the correct bending stress distribution in an intact laminate prior to delamination.

Explicit finite element codes are conditionally stable. The minimum time step that can be used to stably integrate the governing equations is associated with the highest eigenvalue (vibrational mode) in the mesh. The penalty parameter (i.e. spring constant) must be chosen in a judicial manner to avoid adversely impacting the stable time increment. For this reason, the smallest, physically reasonable value for the penalty parameters is used. Recall that K_n penalizes normal displacement across the connection plane. Since the shell elements are transversely inextensible, the estimate for K_n is based on the transverse stiffness of the material between the nodes defining the upper and lower sublaminates.

$$K_n = A\bar{K}_n \qquad where \qquad \bar{K}_n = \frac{E}{h} \tag{1}$$

where E is the sublaminate's transverse Young's modulus, A is the portion of the connection plane area assigned to the node, and h is the sublaminate thickness. Prior to delamination, the displacement ΔU_j is associated with through-the-thickness laminate deformation. When a shear deformable shell is used, the K_t estimate is based on the shear stiffness of a thin, resin-rich layer between sublaminates.

$$K_t = A\bar{K}_t \qquad where \qquad \bar{K}_t = \frac{G^*}{h^*} \tag{2}$$

where G* is the shear stiffness that corresponds to a resin-rich layer (e.g., epoxy shear modulus),

and h* corresponds the thickness of a resin-rich layer (e.g., one quarter of a lamina thickness). Previous work has shown that these choices for penalty parameters lead to an energy release rate, compliance, and stress distribution ahead of the delamination that are in good agreement with detailed finite element results [9]. Note that it is convenient to use area weighted penalty parameters $\overline{K}_n$ and $\overline{K}_t$ as input quantities since they do not depend on element size.

Delamination failure is assumed to initiate at a specified value of the relative displacement across the connection plane. Mode I failure initiates at a critical value of ΔU_j, and mode II failure initiates at a critical value of ΔV_j. Differences in the initiation of mode I and II delaminations can be modeled by specifying different critical values for mode I and II. Though not considered in the present study, a mixed-mode delamination criterion that is a function of both ΔU_j and ΔV_j could be defined. Note that this failure criterion is equivalent to a critical stress criterion. Connection plane stresses F_n/A and F_t/A, where A is the portion of the connection plane area associated with a node, are directly related to ΔU_j and ΔV_j (see Figs. 1 and 2 and Eqs. 1 and 2).

Failure does not occur instantaneously, and energy is dissipated as the delamination grows. Accordingly, the dependence of interfacial stress on separation distance is prescribed, and this defines the gradual reduction in the penalty parameter (Fig. 3). The curve's initial slope is set equal to the $\overline{K}_n$ value given by Eq. 1. The value of $\overline{K}_n$ begins to decrease once $\Delta U_j > U_{crit}$, and continues to decrease until $\Delta U_j = U_{max}$. A linear decrease in the stress-separation relation for $\Delta U_j > U_{crit}$ is a reasonable choice.The reduction in the penalty parameter K_t with mode II separation is defined in an analogous way. In the present implementation, there is no distinction between mode II and mode III delamination growth. The initiation of delamination growth and subsequent separation are based on the vector magnitude of the penalized tangential displacement components. Note that a complete separation in mode I implies a complete loss of resistance to a mode II loading, and vice versa. Interpenetration of the sublaminates is prevented by reapplying the transverse stiffness K_n whenever the delamination closes (i.e., acts like a gap contact element). A mode II

delamination can grow while the delamination is closed in mode I.

The stress-separation relation defined in Figure 3 is like that used in cohesive zone fracture models (see Barenblatt [10] for cracks in homogeneous materials, and Needleman [11] for decohesion along an interface). Accordingly, the separation forces acting between opposing nodes in this discretized formulation can be thought of as defining a cohesive fracture zone. Again consider mode I response, recognizing that mode II-III response is defined in an entirely analogous manner. Since the initial penalty parameter is chosen to represent transverse laminate stiffness (see Eq. 1), ΔU_j values of less than U_{crit} are associated with laminate through-the thickness strain. Only ΔU_j values from U_{crit} to U_{max} are associated with material separation, and the area under this portion of the curve equals the work of separation (i.e., energy dissipated/unit area of delamination growth). Note that the stress-separation relation contains an intrinsic material length scale, U_{max}, and that the energy dissipation/unit area of delamination growth does not depend on element length (sublaminate thickness is assumed to be constant). This avoids the problem of the element size setting the length scale, and leads to mesh independent results provided that the element size is sufficient to define the length of the cohesive zone. Furthermore, the energy release rate for mode I (II) delamination extension equals the area under the mode I (II) stress-separation curve (work of separation) when the sublaminates are linear elastic, inertial effects are negligible, and small scale yielding conditions apply (see Rice [12]). In this case, a mode I delamination propagates at a fixed energy release rate, G_{Ic}.

$$G_{IC} = \frac{1}{2}\bar{K}_n U_{CRIT}(U_{MAX} - U_{CRIT}) \qquad (3)$$

The mode I stress-separation in Figure 3 is not uniquely defined by a G_{IC} value, and either U_{crit} or U_{max} must also be specified. U_{crit} is associated with the critical stress level for the initiation of delamination (separation), while U_{max} is related to the length of the cohesive zone.

Implementation Issues

The delamination modeling technique described in the previous section has been implemented in a three dimensional, transient dynamics, finite element code (PRONTO3D [8]). A special, eight-noded hex element was created to enforce the constraints penalizing the relative displacement across the connection plane between sublaminates. This element is referred to as the DLAM element. The DLAM element looks like, and is meshed like a standard hex element, but it has no mass. It does not use shape functions. It shares nodes with opposing sublaminate shell elements and uses these nodal displacements and rotations to determine the nodal forces and moments needed to make the opposing shell elements act as a single shell element until the connection is broken (see Figs 1 and 2). Implementing the constraints within the context of a hex element provides a natural way for simultaneously accessing the displacement and rotational degrees of freedom of the opposing upper and lower sublaminate shell elements. It also automatically includes the constraint forces when nodal forces are assembled. Other advantages of this approach include: 1) consistency with vector processing of element/material blocks, 2) ease of definition using existing mesh generators; the DLAM hex fits "in between" the sublaminate shell elements and shares the same nodes, and 3) a capability for modeling laminates containing multiple delaminations with sublaminates of differing thicknesses (e.g. shell-DLAM-shell-DLAM-shell). The DLAM element can be used with any type of four node quadrilateral shell element as long as the shell element is defined in terms of the usual displacement and rotational degrees of freedom. Layered shells can be used to model the sublaminates, and there are no restrictions on the type of material model used to model sublaminate response. In particular, material models that include damage and failure can be used.

The penalized relative displacements and the associated constraint forces and moments must be defined with respect to a suitable connection plane coordinate system. Note that the initial shape of a DLAM hex element is not necessarily rectangular, and regardless of its initial shape,

the DLAM hex can be deformed in an arbitrary manner. It is convenient to define a local coordinate system for each of the four DLAM element edges that connect the nodes on the upper and lower sublaminate shells. Consider one of these four DLAM element edges. The first coordinate axis is directed along this DLAM edge. This is the direction of normal relative displacement across the connection plane (i.e., ΔU_j in Fig. 1). The other two local coordinate axes lie within a plane perpendicular to the first axis and are defined with respect to the DLAM element edges that lie in the plane of the sublaminate shells. This coordinate system is continually updated as the DLAM hex deforms. The normal constraint force is always directed along a line connecting upper and lower nodes. This is necessary to avoid artificial stiffening when the laminate is bent.

The minimum time step used for the explicit time integration of the governing equations depends on the highest eigenvalue (vibrational mode) in the mesh. The presence of DLAM elements in a mesh can introduce or modify high frequency vibrational modes. For this reason, formulae have been derived to estimate the frequency of those vibrational modes that might impact the choice of the stable time increment. These estimates are based on simple idealizations that capture the main features of the mode of interest. A through-the-thickness vibrational mode exists when two sublaminates are connected together by springs restraining relative normal displacements. A two mass, one spring system is used to estimate this frequency. The frequency depends on the mode I penalty parameter (stiffness) K_n. The highest extensional (membrane) vibrational frequency of sublaminates joined by a DLAM element is greater than that of the individual sublaminates. When the sublaminates are vibrating 180^o out of phase, the mode II connection (with stiffness K_t) is stretched. This effectively increases the sublaminates extensional stiffness; more force is required to extend the sublaminate. The frequency estimate is based on a bar's natural frequency using a stiffness that includes the effect of the mode II connection. The highest vibrational frequency associated with sublaminate transverse shear stiffness is also increased when a DLAM element connects the sublaminates. A satisfactory estimate for a shell's highest shear frequency is the eigenvalue of the lumped mass-shear stiffness matrix for a linear beam element [13]. When a

DLAM element is present, the shear stiffness matrix must include the rotation-induced contribution to the moment generated by the mode II DLAM connection.

Examples

Calculated results for double cantilever beam (DCB, mode I) and end notched flexure (ENF, mode II) E-glass composite specimens are presented and compared to corresponding test results. This polyester matrix composite is reinforced with a basket weave fabric that is woven from ~ 5 mm wide rovings. Since the composite contains a clearly defined length scale, finite element meshes with comparable element size (5 by 6.25 mm) are used unless indicated otherwise. The fracture specimens analyzed in the present study developed no significant in-plane damage. Accordingly, the sublaminates are modeled as linear elastic materials with a Young's modulus of 30 GPa, and a Poison's ratio of 0.10. Note that reported experimental results are for a quasistatic loading condition. A much faster loading rate (500 mm/s) is used in the analysis to reduce the number of time steps required to complete the calculation. Nevertheless, trial calculations showed that inertia effects are negligible at this loading rate, and the calculated results are applicable to a quasistatic loading. Finally note that the initial values for the area weighted penalty parameters are based on Eqs. 1 and 2, and $\overline{K}_n$=2 kN/mm^3 while $\overline{K}_t$=10 kN/mm^3.

The DCB specimen geometry is defined in Figure 4a. Calculated results for a propagating delamination are in good agreement with experiment when G_{IC} = 0.6 kJ/m^2 and U_{max}=0.30 mm (U_{crit}=0.002 mm) As observed in the tests, the analysis predicts that the delamination grows stably with increasing load point displacement (Fig. 4). Figure 5 compares the calculated load vs. load point displacement relation with results from three DCB tests. As is common practice in a DCB test, the specimen was loaded until the delamination extended about 10 mm, and then unloaded to measure the specimen compliance. This procedure was repeated until the delamination was roughly 100 mm long. For clarity, the unloading curves are removed from the plotted test data, and the remaining portions are associated with a propagating delamination. Test results for

the initial peak load show considerable variation between the three tests. The delamination growth was initiated from an artificially induced delamination. The variability in the measured peak load suggests variability in the character of the inserted flaw and in the initiation of delamination growth from this flaw. After the first unloading, the measured data for the three tests are quite consistent, and the calculated result is in excellent agreement. Visual observations made during the DCB tests identified the presence of partially failed material spanning the delamination plane behind the delamination front [14]. This observation is consistent with the use of a cohesive zone failure model. A cohesive zone length of ~10 mm is predicted for the $U_{max} = 0.3$ mm value used in the analysis (cohesive zone length defined by the number of nodal pairs subjected to a separation force that spans the delamination as it grows). The calculated load vs. crack length relation also in good agreement with the test data (Fig. 6). Note that calculated results are presented for a coarse and a refined mesh in Figures 5 and 6. One calculation uses elements that are 5 mm long by 6.25 mm wide, while the other calculation uses a mesh with elements that are 2.5 mm long by 3.125 mm wide (sublaminate thickness is fixed at 3.1 mm in both calculations). The calculated results are essentially independent of the element's in-plane dimensions. As discussed above, this mesh size independence is an expected consequence of using a cohesive zone fracture model that is defined by a stress-separation relation. Finally note that it is difficult to identify a unique stress-separation relation using the sort of data typically measured during DCB tests.

Figure 7 defines the ENF specimen analyzed. The lower supports are fixed, and the upper load ram is displaced downward. Frictionless contact between the supports, load ram, and specimen are maintained using PRONTO3D's general capabilities to enforce interpenetrability conditions between specified materials [15]. As shown in Figure 8, the calculated result for $V_{crit} = 0.00125$ mm and $V_{max} = 0.25$ mm is in good agreement with the test data. This choice for the stress-separation relation produces a relatively long cohesive fracture zone (~15-20 mm) and high energy dissipation (1.6 kJ/m^2). Typical ENF test results for unidirectionally reinforced composites display an abrupt load drop as the delamination propagates. This behavior is consistent with analytical

results that show that the energy release rate increases as the delamination begins to extend for the usual test configuration[16]. Note, however, delamination growth in the this fabric reinforced composite did not occur in an abrupt, unstable way. Measured load vs. load point displacement relations show that a roughly constant load is maintained once delamination growth is initiated. Calculations that use a lower G_{IIC} and V_{max} value do show an abrupt load drop (Fig. 8).

Summary

A method for modeling the initiation and growth of discrete delaminations in shell-like composite structures has been developed and implemented in a three-dimensional finite element code that uses explicit time integration to advance the equations of motion. This approach uses a special, eight-noded hex constraint element to connect opposing sublaminate shell elements and makes them act as a single shell until a prescribed failure criterion is satisfied. When the failure criterion is reached, the connection is broken, and a discrete delamination is initiated or grows. This method of analysis has been applied to double cantilever beam and end notched flexure fracture specimens. Calculated results were compared to measured data, and the present approach reproduces test results for a propagating delamination. Finally, note that this method of modeling composite delamination can be readily extended to adhesively bonded joints and bonded reinforcements (e.g. doublers and patches). The adhesive bond is modeled with DLAM elements, and the adherends are modeled with shell elements.

References

1. Valisetty, R.R. and Rehfield, L.W. (1985). "A New Ply Model for Interlaminar Stress Analysis," *Delamination and Debonding of Materials, ASTM STP 876*, W.S. Johnson, Ed., pp. 52-68.

2. Chatterjee, S.N. and Ramnath, V. (1988). "Modeling Laminated Composite Structures as Assemblage of Sublaminates," *Int. J. Solids Structures*, Vol. 24, pp. 439-458.

3. Armanios, E.A. and Rehfield, L.W. (1989). "Sublaminate Analysis of Interlaminar Fracture in Composites: Part I-Analytical Model," *J. Comp. Tech. and Res.*, Vol. 11, pp. 135-146.

4. Flanagan, G. (1993). "A Sublaminate Analysis Method for Predicting Disbond and Delamination Loads in Composite Structures," *J. Reinforced Plastics and Composites*, Vol. 12, pp. 876-887.

5. Sankar, B.V. and Hu, S. (1991). "Dynamic Delamination Propagation in Composite Beams," *J. of Comp. Matls.*, Vol. 25, pp. 1414-1426.

6. Farley, G.L. and Jones, R.M. (1992). "Prediction of the Energy-Absorption Capability of Composite Tubes," *J. of Comp. Matls.*, Vol. 26, pp. 388-404.

7. Song, S.J., and Waas, A.M. (1994). "A Spring Foundation Model for Mode I Failure of Laminated Composites Based on an Energy Criterion," *J. Engng. Matl. Tech.*, Vol. 116, pp. 512-516.

8. Taylor, L.M., and Flanagan, D.P. (1989). "PRONTO3D-A Three Dimensional Transient Solid Dynamics Program," SAND87-1912, Sandia National Laboratories, Albuquerque, NM.

9. Dunn, M.L., Reedy, E.D., Jr. and Guess, T.R. (1994). "Delamination of E-Glass/Polyester Woven-Fabric Composites," *Proc. 39th Intl. SAMPE Symposium.*, April 11-14, Anaheim, CA, pp. 1224-1236.

10. Barenblatt, G. I. (1962), "Mathematical Theory of Equilibrium Cracks in Brittle Fracture," *Advances in Applied Mechanics*, Vol. 7, Academic Press.

11. Needleman, A. (1987), "A Continuum Model for Void Nucleation by Inclusion Debonding," *J. Appl. Mech.*, Vol. 54, pp. 525-531.

12. Rice, J. R. (1968), "A Path Independent Integral and the Approximate Analysis of Strain Concentration by Notches and Cracks," *J. Appl. Mech.*, Vol. 35, pp. 379-386.

13. Hughes, T.J.R., Cohen, M., and Haroun, M. (1978). "Reduced and Selective Integration Techniques in the Finite Element Analysis of Plates," *Nucl. Eng. Design*, Vol. 46, pp. 203-222.

14. Guess, T.R., Reedy, Jr., E.D., and Stavig, M.E. (1995). "Characterization of E-Glass/Polyester Woven Fabric Composite Laminates and Tubes," SAND95-2352, Sandia National Laboratories, Albuquerque, NM.

15. Heinstein, M.W., Attaway, S.W., Swegle, J.W., and Mello, F.J. (1993). "A General-Purpose Contact Detection Algorithm for Nonlinear Structural Analysis Codes," SAND92-2141, Sandia National Laboratories, Albuquerque, NM.

16. Carlsson, L.A., and Pipes, R.B. (1987). *Experimental Characterization of Advanced Composite Materials,* Prentice-Hall.

Figure Captions:

Fig. 1. Approach used to connect shells by penalizing normal (mode I) displacement across the connection plane (looking only at left hand side nodes). 1a) relative normal displacement across the connection plane, 1b) force acting on the connection plane, 1c) equivalent nodal force.

Fig. 2.Approach used to connect shells by penalizing tangential (mode II) displacement across the connection plane (looking only at left hand side nodes). 2a) relative tangential displacement across the connection plane, 2b) force acting on the connection plane, 2c) equivalent nodal force and moment.

Fig. 3. Mode I stress-separation relation.

Fig.4. Double cantilevered beam analysis (all dimensions in mm). 4a) DCB geometry, sublaminates 3.1 mm thick, 4b) Time = 0.0175 s, delamination length = 60 mm, and 4c) Time = 0.0350 s, delamination length = 90 mm.

Fig. 5. Comparison of calculated double cantilevered beam load vs. load point displacement relation with test data.

Fig. 6. Comparison of calculated double cantilevered beam load point displacement vs. delamination length relation with test data.

Fig. 7. End notched flexure geometry, sublaminates 3.06 mm thick (all dimensions in mm).

Fig. 8. Comparison of calculated end notched flexure load vs. load point displacement relation with test data.

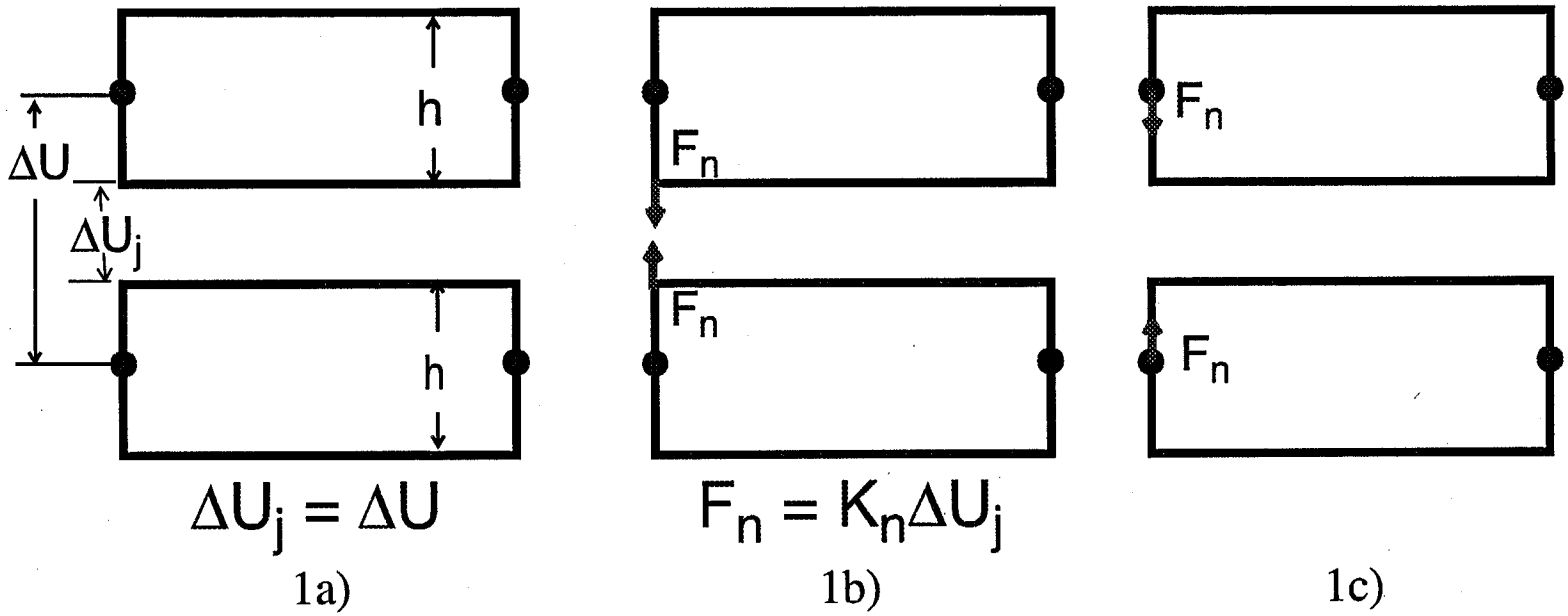

Fig. 1. Approach used to connect shells by penalizing normal (mode I) displacement across the connection plane (looking only at left hand side nodes). 1a) relative normal displacement across the connection plane, 1b) force acting on the connection plane, 1c) equivalent nodal force.

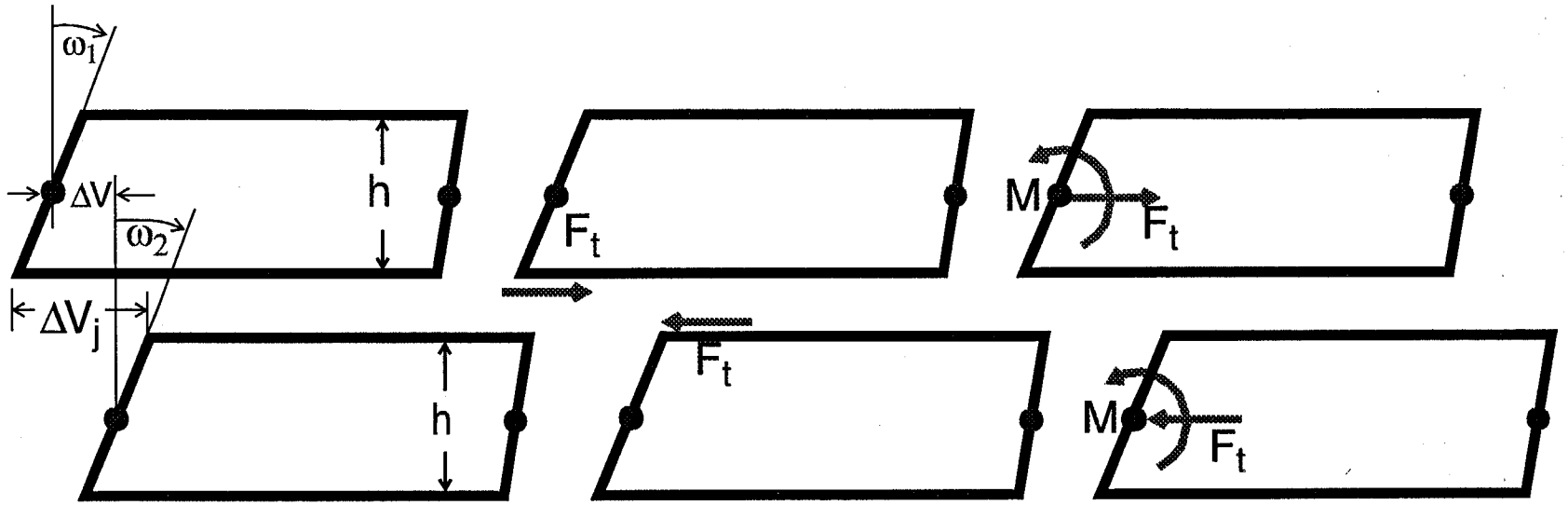

$$\Delta V_j = \Delta V - (h/2)(\omega_1+\omega_2) \qquad \text{2a)}$$

$$F_t = K_t \Delta V_j \qquad \text{2b)}$$

$$M = (h/2)\, F_t \qquad \text{2c)}$$

Fig. 2. Approach used to connect shells by penalizing tangential (mode II) displacement across the connection plane (looking only at left hand side nodes). 2a) relative tangential displacement across the connection plane, 2b) force acting on the connection plane, 2c) equivalent nodal force and moment.

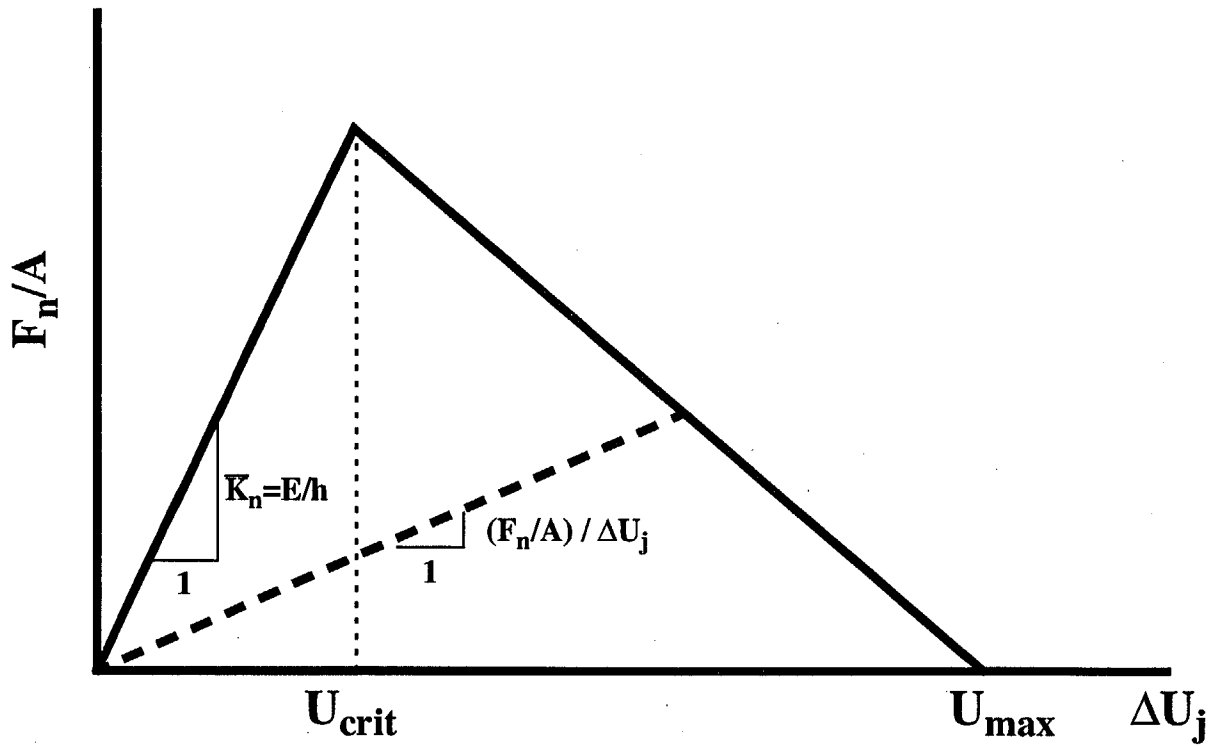

Fig. 3. Mode I stress-separation relation.

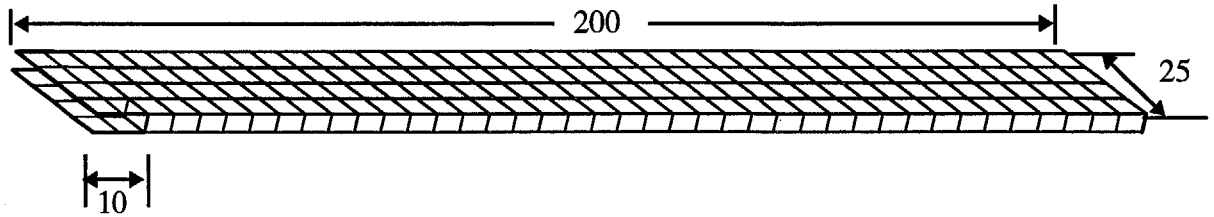

4a) DCB geometry, sublaminates 3.1 mm thick.

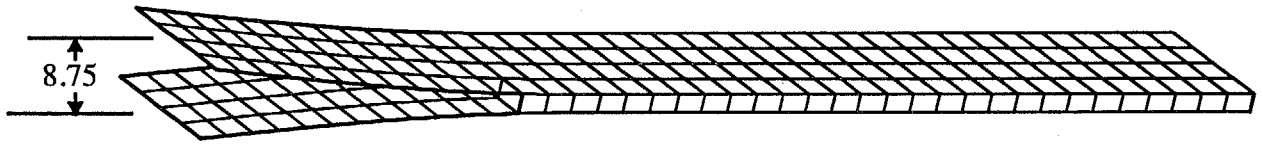

4b) Time = 0.0175 s, delamination length = 60 mm.

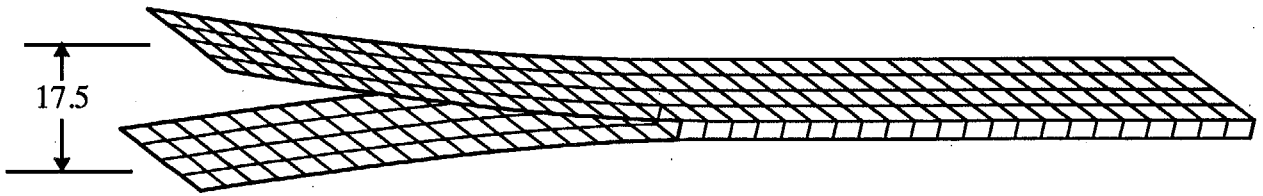

4c) Time = 0.0350 s, delamination length = 90 mm.

Fig. 4. Double cantilevered beam analysis (all dimensions in mm).

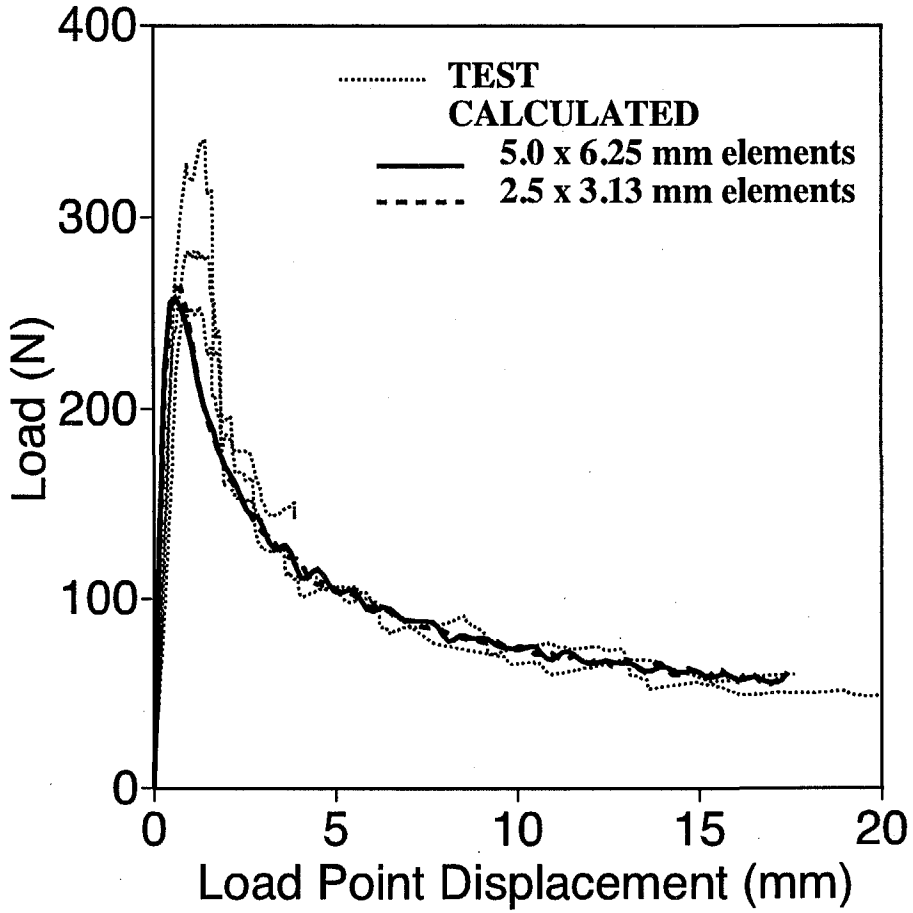

Fig. 5. Comparison of calculated double cantilevered beam load vs. load point displacement relation with test data.

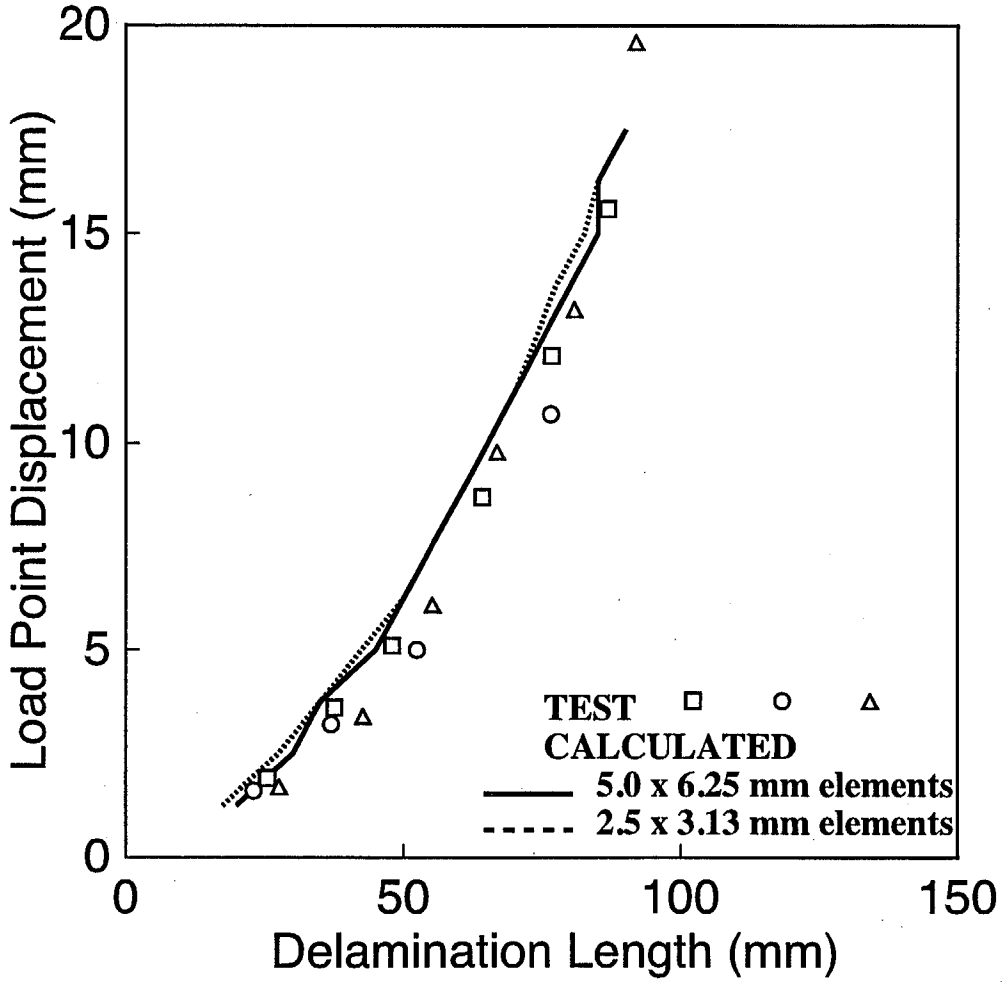

Fig. 6. Comparison of calculated double cantilevered beam load point displacement vs. delamination length relation with test data.

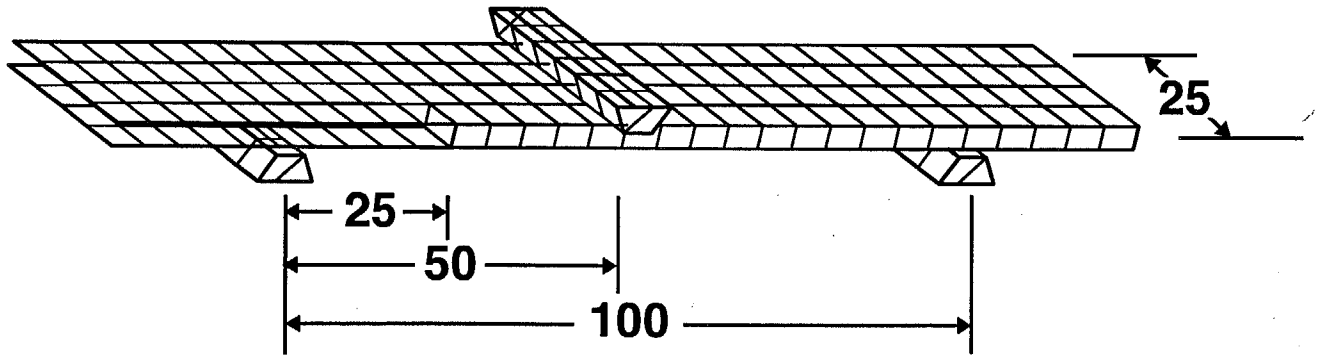

Fig. 7. End notched flexure geometry, sublaminates 3.06 mm thick (all dimensions in mm).

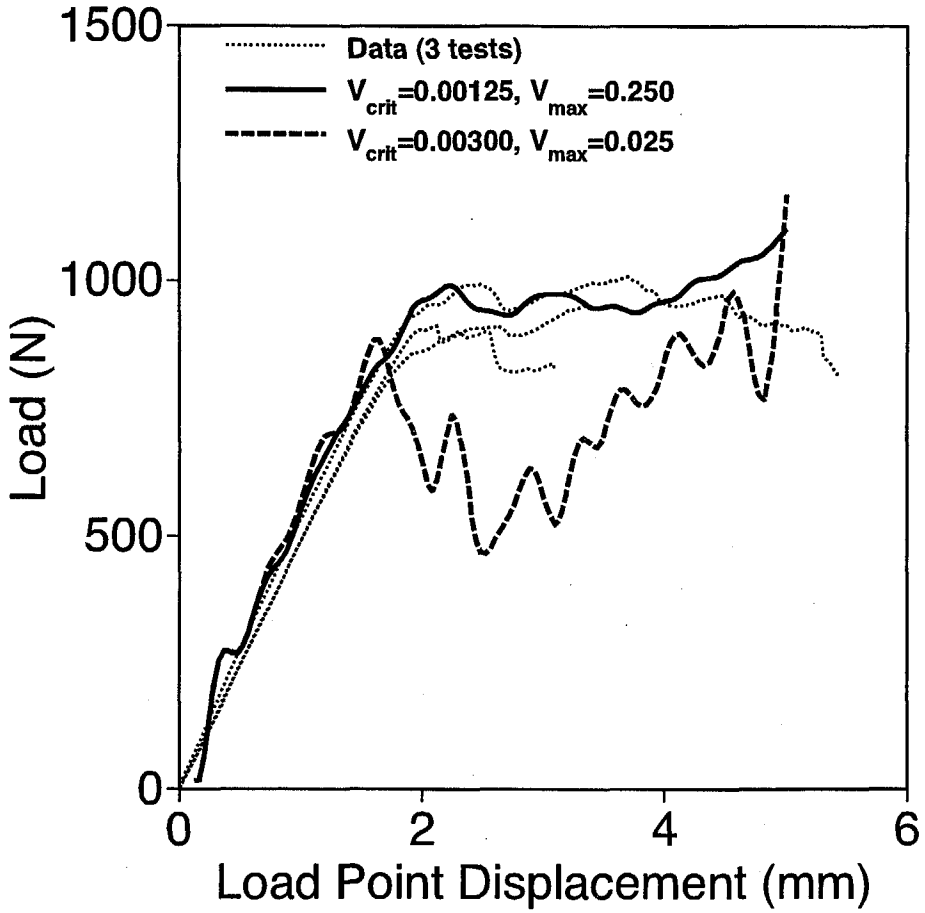

Fig. 8. Comparison of calculated end notched flexure load vs. load point displacement relation with test data.